A Semi-Empirical Model for Electroabsorption in GaAs/AlGaAs Multiple Quantum Well Modulator Structures

G. LENGYEL, SENIOR MEMBER, IEEE, KEVIN W. JELLEY, MEMBER, IEEE, AND REINHART W. H. ENGELMANN, SENIOR MEMBER, IEEE

Abstract—**A semi-empirical model for electroabsorption in GaAs/AlGaAs quantum wells is proposed which is simple and has sufficient accuracy to make it suitable as a fast design-tool for multiple quantum well (MQW) optical modulators. The model is based on a higher order perturbation approach which includes all bound solutions of the unperturbed Hamiltonian. To complete the model, semi-empirical relationships are set up for both the zero-field absorption peak and the half-width at half-maximum (HWHM) values of the heavy-hole (hh) exciton. Comparison with extensive experimental data show a remarkable agreement for a range of wells between 5 and 20 nm and for photon energies on the long wavelength side of the absorption peak. These wavelength and well-size ranges coincide with those needed for practical design.**

I. Introduction

MODERN electroabsorption-type optoelectronic devices most often employ p-i-n epitaxial structures in which the optically active component consists of an intrinsic (i) region composed of alternating layers of very thin (on the order of 10 nm) nominally undoped GaAs well-layers and $Al_xGa_{1-x}As$ barrier-layers. As the bandgap of $Al_xGa_{1-x}As$, which has a lattice constant nearly identical to that of GaAs, is larger than that of the well, a modulation of the energy bands ensues in the direction of layer-growth. This difference in energy gap between well and barrier confines the motion of electrons in the conduction band and of holes in the valence band, more or less, to the plane of the layers, giving rise to interesting quantum effects. The layered crystal is often referred to as a multiple quantum well (MQW) structure. A comprehensive survey on the QW as it pertains to optoelectronics has been given previously by Okamoto [1].

In this paper, we consider uncoupled wells with barriers of sufficient width so as to separate the wells from each other. Thus the wells can be treated as individual entities. Fig. 1(a) shows the schematical band-diagram of such a QW. The confinement of the carriers in the well results in discrete energy levels. In the valance band, one actually obtains two such sets of levels due to the different effective masses of heavy and light holes. The fundamental optical transition occurs between the highest heavy-hole and lowest electronic state which is allowed only for photons polarized to the layers. As most optoelectronic devices utilize this fundamental absorption edge, we shall be concerned only with this transition.

If an electric field is applied perpendicularly to the layers the bands tilt due to the potential of the external field resulting in the shifting of the energy levels [see Fig. 1(b)]. This results in a smaller absorption energy and the absorption edge shifts to longer wavelengths, similar to the Franz-Keldysh effect known from bulk materials. Contrary to the Franz-Keldysh effect, however, the absorption edge retains its steep rise and excitonic character. This phenomenon in QW's is referred to as the quantum confined Stark effect (QCSE) [2]-[5]. It is this steep rise of the absorption edge coupled with a very high excitonic absorption peak which makes this effect so attractive for optoelectronic modulators.

There is an increasing number of device applications in which the QCSE is employed. Fast and efficient optical intensity modulation has been demonstrated in transverse modulators, where the light propagates perpendicularly to the well layers (along the z axis allowing only TE polarization) and in waveguide modulators where the light is guided parallel and along the MQW layers (allowing for both TE and TM polarizations) [6], [7]. Optical bistability was obtained in the QW self-electrooptic effect device (SEED) [8], and recently, a 2 × 2 electrically-driven MQW optical switch has been demonstrated [9].

The theoretical aspects of the QCSE have been extensively treated in the literature and methods have been described to calculate the shift of the hh-exciton peak with an electric field applied in the z direction. [2]-[5] The wave functions are usually separated into a z dependent and a transverse part, with the z part containing the features of the potential well and its modification by the applied electric field. Exact solutions are given as Airy functions for the case of infinitely deep wells and a correction to the well-width renders this solution also applicable to

Manuscript received July 11, 1989; revised August 25, 1989.

G. Lengyel was on leave at the Research Laboratories, Siemens A. G., Munich, West Germany. He is now with the Department of Electrical Engineering, University of Rhode Island, Kingston, RI 02881.

K. W. Jelley is with Siemens Corporate Research, Princeton, NJ 08540.

R. W. H. Engelmann was with Siemens Corporate Research, Princeton, NJ 08540. He is now a Consultant at RR2, Box 209B, Federal City Rd., Pennington, NJ 08534.

IEEE Log Number 8932621.

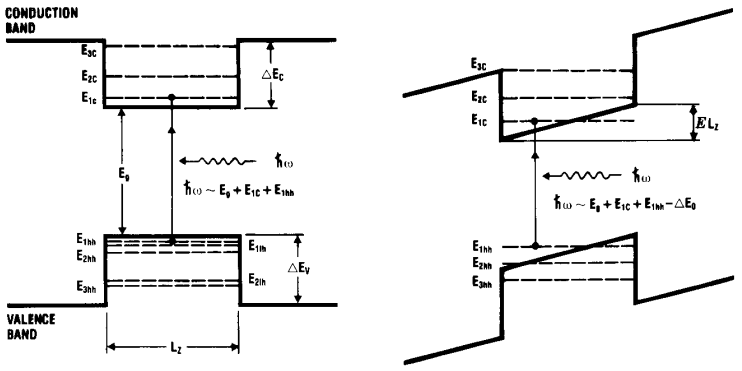

(a) (b)

Fig. 1. Energy band diagram of a single QW. (a) Without external field. (b) With external field.

wells of finite depth [10]. Another technique frequently used is called "tunneling resonance," where a maximum in transmission through the potential well is sought [11].

In this paper, a different method of calculation was employed. Its purpose was not to provide new theoretical insights or to improve the accuracy of other methods. It was found desirable to develop a relatively simple and fast design-tool for the modeling of transverse or waveguide type devices utilizing the QCSE. The desired end result of such a calculation is the knowledge of the absorption edge, $\alpha(\mathcal{E}, h\nu)$ as a function of the applied field $\mathcal{E}$. The model is based partly on theoretical calculations and partly on experimentally measured parameters, namely, the absorption peak of the hh-exciton at zero field and its half-width at half-maximum (HWHM) measured on the low-energy side of the resonance. Using this model, very good agreement was achieved between calculated and measured values of the position and strength of the hh-exciton absorption peak as a function of applied field for well-thicknesses of practical interest.

II. The Analytical Model

A. Determination of Energy Levels and Wave Functions

The QCSE was analyzed using a perturbation method identical to the model described by Yamamoto, Asuda, and Suematsu [12]. There, the potential of the applied field ($\pm e\mathcal{E}z$) is considered as a perturbation of the Hamiltonian and the perturbed wave functions are expressed as a linear combination of unperturbed wave functions. The latter ones are the bound solutions of a particle in a finite potential well. Restricting the expansion to bound states implies the omission of any tunneling effects. Furthermore, the electron–hole excitonic binding energy was also neglected in the Hamiltonian.

Schrödinger's equation for the unperturbed potential well of Fig. 1(a) can be written for the electrons (e) and holes (h) as

$$-\frac{\hbar^2}{2m^*_{e,h}}\frac{d^2\psi^0_{e,h}}{dz^2} + V_{e,h}(z)\psi^0_{e,h}(z) = E_{e,h}\psi^0_{e,h}(z) \quad (1)$$

where $V_{e,h}(z)$ is the potential of the finite well determined by the energy discontinuity between well and barrier materials. In the GaAs/AlGaAs system, this discontinuity can be expressed as $1.247x_{\mathrm{Al}}$[eV] at $T = 300$ K and $x_{\mathrm{Al}} < 0.45$ where x_{Al} represents the mole fraction of the Al in the alloy. This discontinuity is then split between conduction and valence bands. A split ratio of 0.6/0.4 was used in this work. The solutions $\psi^0_{e,h}(z)$ of (1) are simple trigonometric functions in the well and exponentials outside the well in the case of bound states. At the interfaces between well and barrier, the discontinuity in effective masses was taken into account as in [13].

With the application of an external field, the potential term in (1) changes to $[V_{e,h}(z) \pm e\mathcal{E}z]$ where the + sign applies to electrons and the − sign to holes. One can consider the $e\mathcal{E}z$ term as a perturbation and use the method of linear combination of unperturbed wave functions. [14] Thus, the solution of the perturbed Hamiltonian is written as a linear expansion of the unperturbed solutions as

$$\psi_{e,h}(z) = \sum_i a_{ie,h}\psi^0_{ie,h}(z) \quad (2)$$

and the task is then to determine the expansion coefficients $a_{ie,h}$. If the summation in (2) included all bound and unbound (continuum) solutions of (1) the solution would be exact. The inclusion of the continuum states however would have complicated the model to a large extent without contributing significantly to the accuracy of a wide range of cases which are of practical interest. Their omission on the other hand, excludes the effect of tunneling of carriers out of the wells which becomes more significant in the case of very narrow (< 5 nm) well widths and very high (> 200 kV/cm) fields. There still remains the question of convergence of the series (2) but this was found to be completely satisfactory in all cases covered by this paper.

Substituting (2) in the perturbed Hamiltonian, one obtains an eigenvalue problem the solution of which yields the perturbed energy levels $E_{ie,h}$ as eigenvalues and the $a_{ie,h}$ as eigenvectors. Both the solutions of (1) and of the

TABLE I

Electron ΔE_c = 240 meV $m_e^* = 0.067 + 0.083\, x_{Al}$			
i	E_i(meV)	Ψ_i^0 for $\lvert z\rvert < L_z/2$	Ψ_i^0 for $\lvert z\rvert > L_z/2$
0	34.21	0.39 cos (0.245z)	0.11 exp ($\pm$0.6z)
1	127.90	0.38 sin (0.474z)	$\pm$0.23 exp ($\pm$0.442z)
2	233.49	0.26 cos (0.64z)	−0.25 exp ($\pm$0.102z)
Heavy Hole ΔE_v = 160 meV $m_{hh}^* = 0.48 + 0.31\, x_{Al}$			
i	E_i(meV)	Ψ_i^0 for $\lvert z\rvert < L_z/2$	Ψ_i^0 for $\lvert z\rvert > L_z/2$
0	−5.75	0.413 cos (0.269z)	0.065 exp ($\pm$1.391 z)
1	−22.86	0.412 sin (0.536z)	$\pm$0.132 exp ($\pm$1.311z)
2	−50.83	0.408 cos (0.799z)	−0.202 exp ($\pm$1.169z)
3	−88.47	0.401 sin (1.055z)	$\pm$0.272 exp ($\pm$0.946z)
4	−132.69	0.381 cos (1.291z)	0.335 exp ($\pm$0.582z)

$x_{Al} = 0.32$.
$L_z = 10.5$ nm.

TABLE II

Electron ΔE_c = 240 meV				
$\mathcal{E}$ (kV/cm)	ΔE_0 (meV)	a_0	a_1	a_2
0	0	1	0	0
20	−0.216	0.999	−0.048	−0.00092
40	−0.862	0.995	−0.095	−0.0036
60	−1.924	0.99	−0.141	−0.0081
80	−3.387	0.983	−0.185	−0.014
100	−5.226	0.974	−0.226	−0.021

Heavy Hole ΔE_v = 160 meV						
$\mathcal{E}$ (kV/cm)	ΔE_0 (meV)	a_0	a_1	a_2	a_3	a_4
0	0	1	0	0	0	0
20	0.996	0.973	0.231	−0.023	−0.0038	0.00025
40	3.689	0.913	0.401	−0.076	−0.013	0.0012
60	7.547	0.85	0.508	−0.137	−0.027	0.0034
80	12.176	0.794	0.574	−0.195	−0.046	0.0068
100	17.338	0.747	0.614	−0.245	−0.066	0.011

$x_{Al} = 0.32$.
$L_z = 10.5$ nm.

eigenvalue problem were obtained numerically. Still, it can be regarded as an advantage to be able to write the perturbed wave functions as sums of simple analytical functions. In solving the eigenvalue problem, only the highest heavy hole and the lowest electronic energy levels and their wave functions were determined because only these determine the absorption edge.

Table I shows the results of a sample calculation for an $L_z = 10.5$ nm thick well in the unperturbed state ($\mathcal{E} = 0$). The energy values are measured from the bottom of the well for electrons and from the top for holes. The wave functions in the table are normalized.

Table II gives the results of the eigenvalue calculations for an applied field range $0 < \mathcal{E} < 100$ kV/cm. The table lists only the shifts in energy levels (ΔE_0) and the normalized expansion coefficients a_i. One can observe the convergence of the series on the rapid decrease of the higher order terms. The total shift of the exciton (ΔE_{exc}) is obtained as the difference in shifts for electrons and holes.

Fig. 2 shows the plot of perturbed wave functions for electrons (a) and heavy holes (b) as obtained for the case of Table II. They have a smooth appearance and the oscillatory character of the higher order unperturbed solutions is not perceptible, indicating that the approximations are adequate.

The results of the perturbation calculations can be used to determine the overlap integrals of electronic and hole wave functions which govern the peak value of the absorption exciton. As the electron and hole are pushed apart by the field, a reduction in oscillator strength with increasing field is expected. The determination of the absorption coefficient and the absorption edge itself will be discussed in the next section.

B. Absorption Coefficient

For the design of optical light modulators utilizing the QCSE, one needs an analytical expression for the fundamental absorption edge as a function of photon energy and

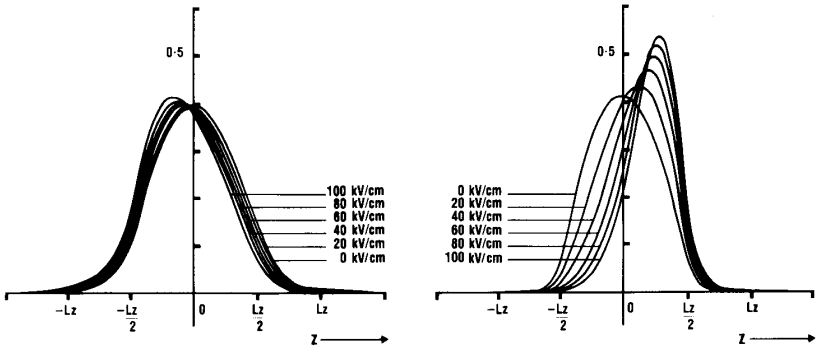

(a) (b)

Fig. 2. Normalized perturbed wave functions of L_z = 10.5 nm well. (a) Electrons. (b) Heavy holes.

applied field. Furthermore, to optimize the effect the well thickness must also be included as a variable.

The optical absorption coefficient can be written as the product of the absorption-exciton peak α_{hh} and a line shape function [15]. The long wavelength side of the absorption edge fits a Lorentzian line shape extremely well according to our measured data, thus the following expression was used for the absorption coefficient:

$$\alpha(\mathcal{E}, h\nu, L_z) = \alpha_{hh}\left\{1 + \left[\frac{(E_0 - h\nu)}{\Gamma_{hh}}\right]^2\right\}^{-1} \quad \text{for } h\nu < E_0 \tag{3}$$

with E_0 the energy of the hh exciton and Γ_{hh} its HWHM. α_{hh} is the peak value of the absorption exciton which depends on the well thickness L_z and applied field $\mathcal{E}$. Furthermore, E_0 and Γ_{hh} are also functions of L_z and $\mathcal{E}$.

The peak value α_{hh} can be calculated from first principles as in [15] but that requires the knowledge of such quantities as the size of the exciton. Instead of following a strictly theoretical way, we retained the analytical dependence on L_z and $\mathcal{E}$ in α_{hh} and the remaining constant of proportionality was determined from the experimental data.

$$\alpha_{hh}(L_z, \mathcal{E}) = \frac{C}{L_z}\left|\int_{-\infty}^{\infty} \psi_e(z)\psi_h^*(z)\,dz\right|^2 + \alpha_{bulk}. \tag{4}$$

The inverse L_z dependence is due to the density of states appearing in the theoretical expression of the transition rate and the overlap integral comes from the transition matrix element. This latter also includes the field dependence of α_{hh} as discussed in Section II-A. The field dependence of α_{bulk} was neglected. The experimental verification of the inverse L_z dependence of our data for well thicknesses above 5 nm was published elsewhere [16]. Very good agreement could be obtained with C = 16 000 nm/cm and α_{bulk} = 5500 cm^{-1}. For well thicknesses below 5 nm, the L_z dependence of α_{hh} contains higher order terms in $1/L_z$ [16], which were neglected in this work as (4) was found adequate for the range considered here.

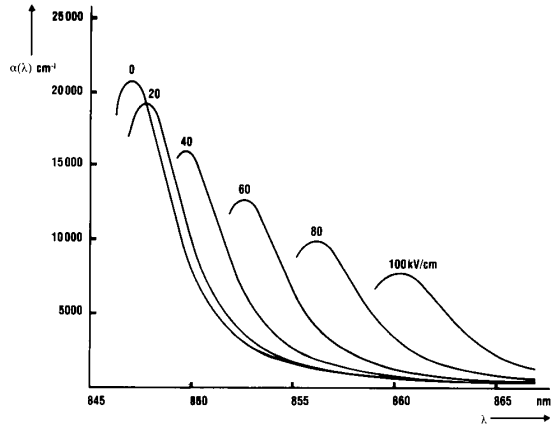

Fig. 3. Calculated absorption edges for L_z = 10.5 nm well.

The dependence of E_0 in (3) on well thicknesses and field was obtained from the perturbation calculation. For the variation of the HWHM Γ_{hh}, we followed the model of Stevens *et al.* [17]. Besides the broadening of the exciton caused by phonons, they included a field-dependent broadening as well caused by small fluctuations in the exciton's energy. These are due to variations in well-thickness and in the electric field.

$$\Gamma_{hh}(L_z, \epsilon) = \Gamma_{hh}(L_z)_{phonon} + \frac{\partial E_0}{\partial \epsilon}\Delta\mathcal{E} + \frac{\partial E_0}{\partial L_z}\Delta L_z. \tag{5}$$

The partial derivatives can be obtained from the perturbation calculation. Instead of using estimates for $\Gamma_{hh\,phonon}$, $\Delta\mathcal{E}$, and ΔL_z, a polynomial expression was fitted to the measured data. Comparing the polynomial with (5), estimates for the fluctuations could be obtained. The polynomial expression used for 5 nm $\leq L_z \leq$ 20 nm was

$$\Gamma_{hh}(L_z, \mathcal{E}) = 7.374 - 0.511\,L_z + 0.0182\,L_z^2 - 0.054\,\mathcal{E} + 0.0161\,\mathcal{E}^2. \tag{6}$$

Γ_{hh} is in meV, L_z in nm, and $\mathcal{E}$ in mV/nm. Comparison with (5) gave 2.5 to 3.5 Å for ΔL_z and 2 to 3 kV/cm for

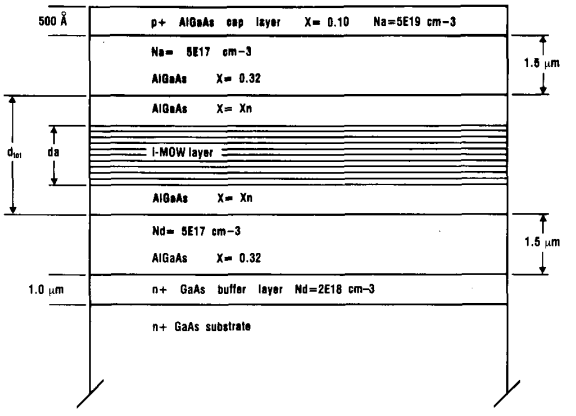

Fig. 4. Schematic of experimental MQW structures.

TABLE III
SAMPLE PARAMETERS BASED ON TEM/SEM/PL MEASUREMENTS

Wafer #	L_z nm	L_b nm	# w	# b	d_w μm	d_a μm	d_{tot} μm	x_b	x_n
A825	4.7	10.5	100	101	0.47	1.53	1.53	0.32	0
A826	7.6	10.5	67	66	0.509	1.20	1.57	0.32	0.32
A661	10.5	9.5	50	51	0.525	1.01	1.01	0.32	0
A662	15.5	9.5	33	32	0.512	0.816	1.00	0.34	0.32
A663	20.5	9.5	25	24	0.513	0.741	1.00	0.33	0.32

L_z = well width.
L_b = barrier width.
#w, #b = number of wells, barriers.
d_w = total thickness of wells.
d_a = total width of wells + barriers.
d_{tot} = total layer thickness.
x_b = Al concentration of barriers.
x_n = Al concentration of neutral i layers.

$\Delta\mathcal{E}$. This latter corresponds to a background doping in the low 10^{15} cm^{-3} range, which is a reasonable value for an MBE material. The actually-measured background doping was found to be 5×10^{14} cm^{-3}. Calculated absorption edges for wavelengths longer than that of the exciton's are plotted in Fig. 3 for the well thickness of 10.5 nm.

III. Comparison with Experiment

The MQW structures were grown by molecular beam epitaxy with well thicknesses ranging from 1.7 to 26 nm. The number of wells was varied in the different samples to give a total well thickness of approximately 0.22 and 0.5 μm. Transmission spectra were measured with the incident light being perpendicular to the layers (polarization parallel to layers). The details of the experiment were described elsewhere [18]. The schematic of the structure is shown in Fig. 4; the data of the sample used in this work are compiled in Table III.

Fig. 5 shows a typical set of measured absorption spectra of the 10.5 nm well thickness. The electric field in the wells was determined from the applied voltage with the known doping profile by solving Poisson's equation (see Fig. 6). The absorption spectra display the characteristic excitonic features of the QCSE. Similar sets of curves were obtained for all the other samples as well. Fig. 7 shows the position of the zero-field exciton, comparing calculated and measured values. The agreement in this case was excellent despite the neglect of the exciton's binding energy. Fig. 8 presents this comparison for the exciton's shift to lower photon energies with applied field. The agreement in this case is within 2 meV for wells of 7.6, 10.5, and 15.5 nm thickness, the deviations for the 4.7 nm sample are larger however. This indicates the limit of the applicability of the model; omission of tunneling and the exciton's binding energy lead to larger errors. It will be discussed later that this limitation is not a very severe one as thicknesses below 5 nm do not bring practical advantages. The shift of the exciton in the 20.5 nm sample could not be measured reliably due to the rapid collapse of the exciton even at relatively low fields. Fig. 9 displays the comparison between the decrease of the exciton's peak value as measured and that of the overlap integrals as calculated from the model. All curves are normalized to the zero-field case. The same conclusions can be drawn here too as from Fig. 8.

In the design of optical modulators, several characteristics of the device are of interest depending on the application. A high absorption change is always desirable, but

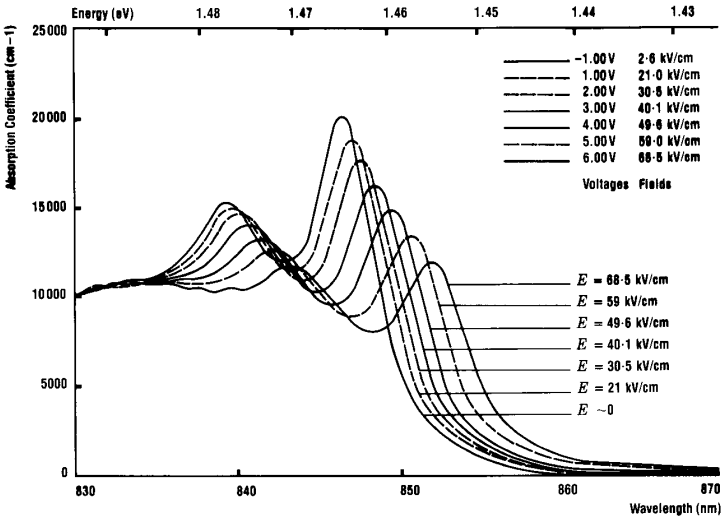

Fig. 5. Measured absorption spectra of sample A661, L_z = 10.5 nm.

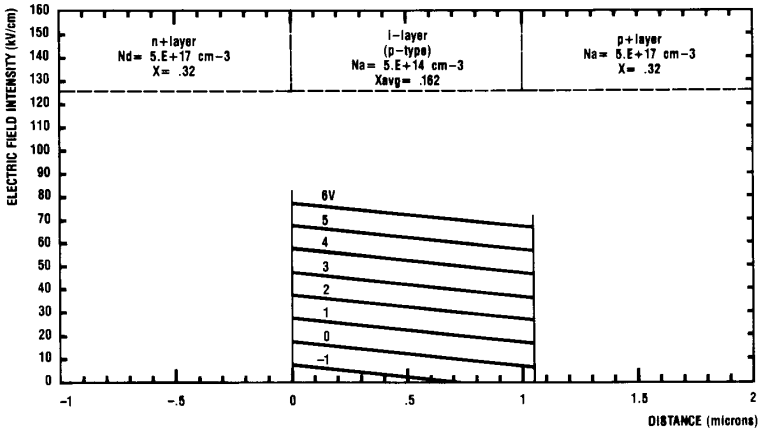

Fig. 6. Calculated field distributions in the *i* region of sample A661.

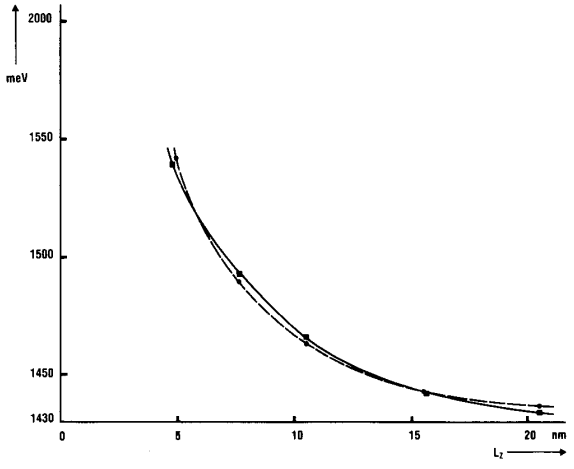

Fig. 7. Heavy-hole exciton energy as a function of well thickness. Experiment: solid line, model calculation: dashed line.

high transmission at zero-field can be equally important. Naturally, these features cannot be looked at independently of each other, as, e.g, a higher absorption change usually results in a shorter device which, in turn, improves transmission at zero field. It is, therefore, appropriate to consider the largest absorption change as a criterion for optimization, as it will be decisive in the design in most cases. It should be, however, emphasized that a particular device optimization might require conditions that deviate from the largest absorption change.

If one computes the absorption edge using (3), (4), and (6), and subtracts the absorption at zero-field, the curves of Fig. 10 are obtained for the 10.5 nm sample. One can see from Fig. 5 that for any photon energy smaller than the exciton's energy there is a maximal change in absorption going from its zero-field value to a higher absorption at some characteristic field value which depends on the photon energy. This field value can also be found by interpolating between curves of the graph. There is a par-

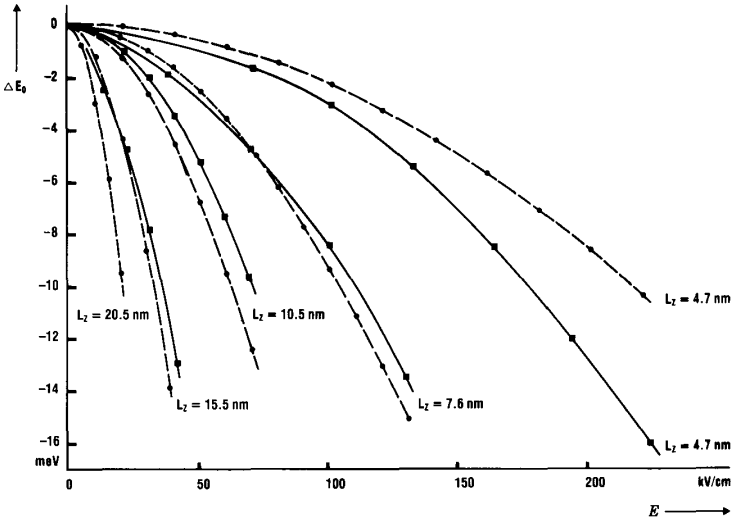

Fig. 8. Shift of hh exciton with applied field. Experiment: solid line, model calculation: dashed line.

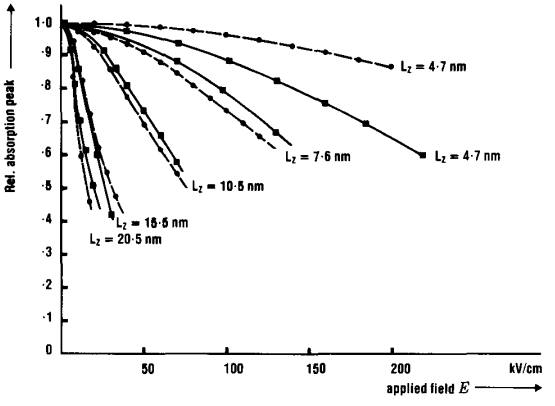

Fig. 9. Decrease of absorption-peak with applied field. Experiment: solid line, overlap-integrals: dashed line.

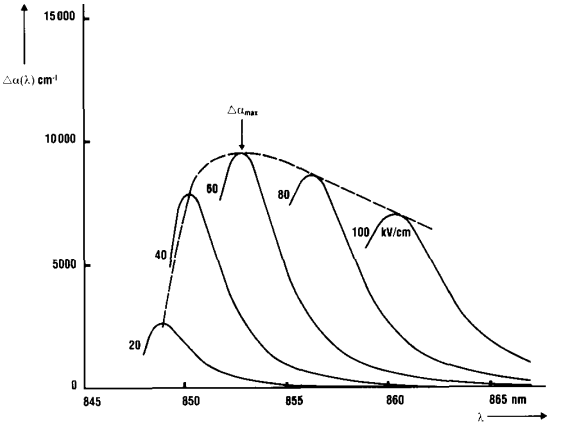

Fig. 10. Calculated absorption change $\Delta\alpha$ for the L_z = 10.5 nm sample.

ticular photon energy $h\nu_{max}$ (or wavelength λ_{max}) at which this change $\Delta\alpha_{max}$ is maximum for any given well thickness. The characteristic field value pertaining to this maximal change is denoted by $\mathcal{E}_{max}$. This triad of values represents an optimal operating condition of the absorption-modulator for a particular value of L_z. These optimal values were determined from the experimental data and of the model and are shown in Fig. 11 as functions of well thickness. The agreement is excellent between 7 and 20 nm. At 5 nm, the measured and calculated curves begin to deviate from each other indicating that the limit of validity of the model has been reached. Although the largest $\Delta\alpha_{max}$ was measured in a 3.5 nm well, it cannot be optimally utilized because the required field strengths become excessively high. Thus, well-thicknesses less than 5 nm are of reduced practical importance. At 20 nm or higher well-thicknesses on the other hand, the exciton's confinement becomes too weak and the behavior of the MQW material begins to resemble that of the bulk. Therefore, one can state that devices subject to the practical constraints of low operating fields would more likely utilize well thicknesses in the 7.5 to 15 nm range for which the simple model presented here provides sufficiently accurate data.

IV. Design Example

As a design example, we wish to quote some results obtained with this model for an integrated laser-EA modulator where the modulator forms part of the laser cavity. This calls for a self-consistent solution of the equations describing the operating parameters of the laser (threshold current, threshold carrier density, emission wavelength) and those of the modulator (absorption coefficient, field strength, and wavelength). These equations are coupled mainly through the wavelength as the optical losses in the modulator are wavelength dependent and, at the same

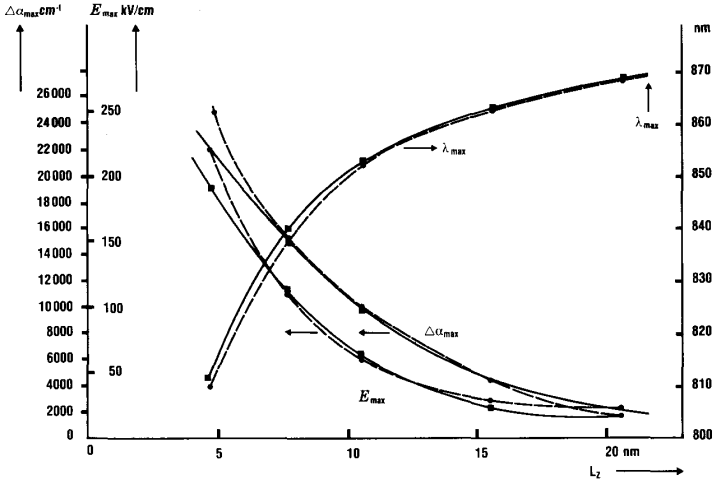

Fig. 11. Optimized operating parameters $\Delta\alpha_{max}$, $\mathcal{E}_{max}$, and λ_{max} of QW modulator as a function of well thickness. Experiment: solid line, model calculations: dashed line.

TABLE IV

	Extinction Radio (db)				Differential Quantum Efficiency (W/A)		
z	L = 10	15	20	z	L = 10	15	20
5	−6.5	−10.9	—	5	0.176	0.14	—
6	−8.0	−13.2	−18.2	6	0.182	0.155	0.124
7	−10.5	−15.4	−21.5	7	0.182	0.159	0.137

L_z = 7.5 nm.
L = length of modulator section in μm.
z = number of QW's.
Laser section: length 400 μm, width 3 μm, MCRW.
Modulator operating field strength: 120–140 kV/cm.

	Extinction Ratio (db)				Differential Quantum Efficiency (W/A)		
z	L = 20	25	30	z	L = 20	25	30
4	−8.8	−13.2	—	4	0.160	0.137	—
5	−11.0	−15.1	−19.7	5	0.165	0.157	0.133
6	−14.1	−18.3	−21.7	6	0.167	0.159	0.137

L_z = 10 nm.
L = length of modulator section in μm.
z: number of QW's.
Laser section: length 400 μm, width 3 μm, MCRW.
Modulator operating field strength: 70–90 kV/cm.

time, these cavity losses affect the threshold carrier density in the laser section. This, in turn, determines the emission wavelength. The model presented in this paper proved to be highly efficient in solving this problem.

In optimizing such a structure, the objective is to find design parameters for the laser and modulator sections in such a way that the resulting operating conditions fall in the vicinity of the optimal triad of values described in the previous section. Table IV lists the obtainable extinction ratios for different modulator lengths and number of QW's in the cases of 7.5 and 10 nm well thicknesses. Extinction ratios in the 15–20 db range can be obtained but the larger values are achieved at the expense of reduced differential quantum efficiency. For comparison, the differential quantum efficiency of the laser section alone without modulator for the assumed MCRW structure was estimated to be 0.22 W/A. The incorporation of the modulator having 20 db extinction ratio cuts the differential quantum efficiency almost in half. Conditions can be improved by increasing the facet reflectivity on the laser end of the integrated device.

V. Conclusions

The design of electrooptical devices utilizing the QCSE in QW's requires knowledge of the fundamental absorption edge and its dependence on the applied electric field.

A simple mathematical model based on a higher order perturbation calculation is presented which gives good agreement with experimental values for the position of the hh exciton, its shift with applied field, and the decrease of the absorption exciton's peak in a range of well thicknesses between 5 and 20 nm. This range also corresponds to values used in practical devices. A semi-empirical expression based on experiments is used to model the absorption coefficient as a function of wavelength, well thickness, and applied field. The optimal operating conditions of a QCSE modulator were determined as a function of well thickness both from the model and from experiments. The agreement in the given range was found to be excellent. A design example of an integrated laser-EA modulator is presented as an illustration of the usefulness of the model.

Acknowledgment

The authors wish to thank K. Alavi and H. Lee for the growth of the samples.

References

[1] H. Okamoto, "Semiconductor quantum-well structures for optoelectronics, recent advances and future prospects," *Japan. J. Appl. Phys.*, vol. 26, pp. 315-330, 1987.

[2] D. A. B. Miller, D. S. Chemla, T. C. Damen, A. C. Gossard, W. Wiegmann, T. H. Wood, and C. A. Burrus, "Band edge electroabsorption in quantum-well structures: The quantum confined Stark effect," *Phys. Rev. Lett.*, vol. 53, pp. 2173-2176, 1984.

[3] ——, "Electric field dependence of optical absorption near the band gap of quantum-well structures," *Phys. Rev. B.*, vol. 32, pp. 1043-1060, 1985.

[4] D. A. B. Miller, D. S. Chemla, and S. Schmitt-Rink, "Relation between electroabsorption in bulk semiconductors and in quantum-wells: The quantum-confined Franz-Keldysh effect," *Phys. Rev. B.*, vol. 33, pp. 6976-6982, 1986.

[5] D. A. B. Miller, J. S. Weiner, and D. S. Chemla, "Electric field dependence of linear optical properties in quantum-well structures: Waveguide electroabsorption and sum rules," *IEEE J. Quantum Electron.*, vol. QE-22, pp. 1816-1830, 1986.

[6] T. H. Wood, "Multiple quantum well (MQW) waveguide modulators ," *J. Lightwave Technol.*, vol. 6, pp. 743-757, 1988.

[7] J. S. Weiner, D. S. Chemla, D. A. B. Miller, H. A. Haus, A. C. Gossard, W. Wiegmann, and C. A. Burrus, "Highly anisotropic properties of single quantum well waveguides," *Appl. Phys. Lett.*, vol. 47, pp. 664-667, 1985.

[8] D. A. B. Miller, A. C. Gossard, and W. Wiegmann, "Optical bistability due to increasing absorption," *Opt. Lett.*, vol. 9, pp. 162-164, 1984.

[9] T. H. Wood, E. C. Carr, C. A. Burrus, J. E. Henry, A. C. Gossard, and J. H. English, "High speed 2 × 2 electrically driven spatial light modulator made with GaAs/Al-GaAs multiple quantum wells (MQW's)," *Electron. Lett.*, vol. 23, pp. 916-917, 1987.

[10] I. J. Fritz, "Energy levels of finite-depth quantum wells in an electric field," *J. Appl. Phys.*, vol. 61, pp. 2273-2276, 1987.

[11] A. Harwit, J. S. Harris, and A. Kapitulnik, "Calculated quasi-eigenstates and quasi-eigenenergies of quantum-well superlattices in an applied electric field," *J. Appl. Phys.*, vol. 60, pp. 3211-3213, 1986.

[12] H. Yamamoto, M. Asuda, and Y. Suematsu, "Theory of refractive-index variation in QW structures and related intersectional optical switch," *J. Lightwave Technol.*, vol. 6, pp. 1831-1840, 1988.

[13] W. Stolz, J. C. Maan, M. Altarelli, L. Tapfer, and K. Ploog, "Absorption spectroscopy on $Ga_{.47}In_{.53}As/Al_{.48}In_{.52}As$ multi quantum well heterostructures. II. Subband structure," *Phys. Rev. B*, vol. 36, pp. 4310-4315, 1987.

[14] H. Margenau and G. M. Murphy, *The Mathematics of Physics and Chemistry*. Princeton, NJ: Van Nostrand, 1956, ch. 11, p. 383.

[15] K. Nishi and T. Hiroshima, "Enhancement of quantum confined Stark effect in a graded gap quantum well," *Appl. Phys. Lett.*, vol. 51, pp. 320-322, 1987.

[16] K. W. Jelley, R. W. H. Engelmann, K. Alavi, and H. Lee, "Well size related limitations on maximum electro-absorption in GaAs/AlGaAs MQW structures," *Appl. Phys. Lett.*, vol. 54, July 1989.

[17] P. J. Stevens, M. Whitehead, G. Parry, and K. Woodbridge, "Computer modeling of electric field dependent absorption spectrum of MQW material," *IEEE J. Quantum Electron.*, vol. 24, pp. 2007-2016, 1988.

[18] K. W. Jelley and R. W. H. Engelmann, "Experimental determination of electroabsorption in $GaAs/Al_{.32}Ga_{.68}As$ MQW structures as function of well width," *Electron. Lett.*, vol. 24, pp. 1555-1557, 1988.

G. Lengyel (M'59-SM'86), photograph and biography not available at the time of publication.

Kevin W. Jelley (M'84-S'84-M'86), photograph and biography not available at the time of publication.

Reinhart W. H. Engelmann (SM'82), photograph and biography not available at the time of publication.